Exploring the effect of underwater burial on the resonant behaviour of simplified shell geometries

Joseph Milton (1), Marshall Hall (2), Yan Kei Chiang (3),
Benjamin Halkon (1), Sebastian Oberst (2) and David Powell (3)

(1) School of Mechanical and Mechatronic Engineering, University of Technology Sydney, Sydney, Australia
(2) Centre for Audio, Acoustics and Vibration, University of Technology Sydney, Sydney, Australia
(3) School of Engineering & Information Technology, University of New South Wales, Canberra, Australia

ABSTRACT

Naval mines and unexploded ordnance litter large areas of the ocean floor resulting in many coastlines being abandoned due to their deadly and indiscriminate threat. Over time, many become buried within the seabed, becoming less visible and thereby presenting a challenge to existing image-based detection techniques. Alternative approaches might rely on acoustic scattering, and it is therefore necessary to understand how the signatures of such objects may change when burial occurs. In this paper, the scattering spectra of several simple shell geometries have been evaluated through complementary but independently developed numerical and analytical modelling techniques. Scenarios investigated include air and fluid-filled spherical targets surrounded either by seawater or saturated sand, representative of burial within the seabed. The results show how embedding the objects within saturated sand results in a decrease in frequency of the dominant scattering resonances. In general, these frequencies were reduced by a factor of between 1.2 and 1.4.

1 INTRODUCTION

Active sonar-based techniques have been widely used for underwater object detection and localisation since the mid 20th century, with application across military, commercial and scientific industries (Bjørnø, 2017). In its most basic form, active sonar projects pulses of sound through the water and captures the reflections scattered by objects to determine their presence (*detection*) and position (*localisation*). With the ever-increasing threat posed by naval mine warfare (Naval Research Council, 2001), mine-like-object (MLO) classification is becoming increasingly important, particularly in the cluttered littoral environment. In recent years, therefore, numerous sonar scanning and processing techniques have been proposed which aim to increase the accuracy of MLO classification (Langner et al., 2009). Typically, such techniques have relied upon high resolution sonar imagery (Le et al., 2020), which utilises high frequency sound waves to exploit the geometrical theory of diffraction and enhance interpretation of the outer shape of the MLO. However, these techniques fail when the MLO is not clearly visible, for example if it has become buried, with high frequency sound waves less effective at penetrating the seabed.

The use of lower frequency pulses (~10 kHz), while able to more effectively penetrate the seabed (Maguer et al., 2000), has the drawback that the wavelength of the pulses is too large to create sufficiently high-resolution sonar images for image-based classification. These frequencies are, however, typically more suitable to excite strongly scattering structural resonances within man-made structures, for example MLOs. This acoustic scattering yields information about the object that can be effectively used for both classification and some degree of identification based on the unique resonant behaviour of the scattering object (Tesei et al., 2000, Flax and Neubauer, 1978). These types of mine countermeasures (MCM) are most effective when a large, reference database of known MLO acoustic scattering responses is available, often used to train computer algorithms. The database is often developed by modelling, typically numerically, potential targets in a variety of configurations, for example, in the water column or embedded within the seabed (Burnett, 2015).

This paper presents a study that compares the scattering spectra of a number of simple shell targets when surrounded by a seawater acoustic domain and a water-saturated sand acoustic domain, which aims to model the effects of underwater burial. The scattering spectra are also evaluated as the properties of the shell's inner domain changes from air, to either seawater or saturated sand, simulating the potential changes that may occur over time due to leaks, or shell deterioration. The purpose of this work is to validate our numerical modelling capability against a well-established analytical approach developed by (Hickling, 1964). Further, this work has also been framed to determine to what extent these changes alter the expected scattering response of specific geometries, with a view to provide insight for experimental work on MLO identification, using similar targets.

2 SCATTERING FROM AIR-FILLED SPHERICAL SHELLS

The scattering from targets suspended in the water column and buried within the seabed is evaluated for three stainless steel spherical shells. This focus on spheres is, in part, because numerical and analytical modelling of such targets and their scattering response is simplified as a result of symmetry and is already well-developed in the literature (Hickling, 1964). Furthermore, future experimental work within this research project will initially utilise similar targets due to their relative ease of availability and deployment. In the following, the modelled scenario is described with both the numerical and analytical models formulated and developed.

2.1 MODELLED ENVIRONMENT AND CONFIGURATION

Three spherical shells were considered, with radii and thicknesses as set out in Table 1. Each has been modelled in free-field conditions, surrounded by homogeneous fluid of either seawater or water-saturated sand, thereby simulating suspension in the water column and burial within the seabed, respectively. All three shells were modelled using 304 stainless steel with Table 2 defining the material properties. The different properties of the two domains considered – seawater and water-saturated sand – are given in Table 3.

Table 1: Geometric properties of spherical shells

Parameter	Sphere $_{50,1}$	Sphere $_{50,0.55}$	Sphere $_{100,1}$
Radius (mm)	50	50	100
Thickness (mm)	1	0.55	1

Table 2: Material properties of 304 stainless steel

Parameter	Value
Young's modulus (GPa)	196
Density (kg/m^3)	7950
Poisson's ratio	0.27

Table 3: Properties of the modelled domains (seawater vs. saturated sand)

Parameter	Seawater	Saturated sand
Density (kg/m^3)	1025	2000
Speed of sound (m/s)	1520	1750
Attenuation (dB/λ)	0	0.83

The inner domains of each shell were modelled as either *Full* or *Empty*. *Full* refers to an inner domain that is the same as the outer domain, therefore, either seawater or saturated sand. *Empty* refers to an inner domain of air, for the numerical model, or vacuous, for the analytical model. Due to the limitations of the analytical model that was used (Hickling, 1964) at the time of writing, it was only possible to analytically model either a vacuous inner domain or match the inner to the outer domain. It was assumed that, at this scale, the vacuous inner domain would be represented in reality by air. This assumption was validated by the results presented in this study, and since writing, further development of the analytical model has also backed up this assumption.

In this study, it was assumed that all spheres are at a constant depth shallower than 100 m since this is the greatest seafloor depth that would likely be considered for submarine mine fields, as mines deeper than this become ineffectual against shallow targets. Within this range (0 to 100 m), the small effect of hydrostatic pressure acting on the sphere can be neglected. As the pressure external to the shell is increased (slowly) by δP, the shell volume (V) changes by an amount δV given by:

$$\delta V / V = - \delta P / B, \tag{1}$$

where B is the shell's bulk modulus. A general expression for B of a fluid-filled solid spherical shell is (Hall, 1975)

$$B = N/D, \tag{2}$$

where:

$$N = mF + (4/3)G[(m-1) + F/K], \tag{3}$$

$$D = 1 + [(m-1)F + (4/3)mG]/K, \tag{4}$$

in which m is the cube of the ratio of the outer and inner shell radii, F is the bulk modulus of the internal fluid, and G and K are the shear and bulk moduli of the shell material. Therefore, for the three vacuous shells listed in Table 1, B is computed to be 3.6, 2.0, and 1.0 GPa, respectively, and the corresponding results for the three air-filled shells are 3.6, 2.0, and 1.8 GPa. As depth increases from 0 to 100 m, hydrostatic pressure in water increases by 1 MPa. For an increase in external pressure of 1 MPa, the radii of Sphere $_{50,1}$ and Sphere $_{50,0.55}$ will thus decrease by no more than 0.02 %, and the radius of Sphere $_{100,1}$ will decrease by 0.02 % if air-filled and 0.03 % if vacuous. The consequent increases in their resonance frequencies will therefore be too small to affect the conclusions of a classification utility.

Finally, a simple monostatic active sonar system was modelled, assuming that both source and sensor were positioned directly above the targets. The outgoing sonar signals were modelled using incident plane waves, ranging from 1 to 20 kHz in steps of 20 Hz, propagating through the outer domain. The back scattering response to each incident wave was evaluated 0.5 m from the target, azimuth relative to the incident wave. In the following two subsections, the numerical and analytical models used to simulate this scenario are described in detail.

2.2 FORMULATION OF THE NUMERICAL MODEL

To investigate the resonant behaviour of the spherical shell geometries using numerical modelling methods, full-wave simulations were performed with COMSOL Multiphysics 5.4. In this study, the scatterers considered are axially symmetric, enabling three-dimensional solutions to be approximated with the reduced computational cost of performing the simulations in a two-dimensional, axisymmetric space. Figure 1 depicts the geometry of the numerical model.
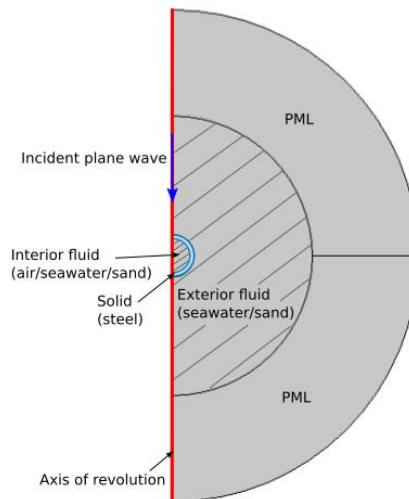

Figure 1: Schematic of half the cross section of the spherical numerical model geometry.

Both the exterior and interior fluid domains were modelled with the Pressure Acoustics, Frequency Domain Module. To enforce the Sommerfeld radiation condition, perfectly matched layers (PMLs) of one wavelength thickness were added to the outer boundaries of simulation domains. The structural behaviour of the spherical shell is modelled by using the Solid Mechanics interface, which is coupled to the fluid domains via the Acoustic-Structure Boundary coupling feature. A plane wave with unity amplitude is applied to create an incident field and the relative pressure spectrum is calculated using the following expression for the relative pressure, p_{rel}:

$$p_{rel} = 20\log_{10}\left(\frac{|p_s|}{|p_{incl}|}\right), \tag{5}$$

where p_s is the scattered pressure evaluated at a single point, 0.5 m from the shell. To ensure the wave physics was accurately resolved, the maximum element size is set to one-tenth of the wavelength of the incident pressure.

This value was chosen as a quick mesh convergence test showed that the model achieved convergence after approximately one-eighth of a wavelength.

2.3 FORMULATION OF THE ANALYTICAL MODEL

To investigate the scattering response of the spherical shell geometries using analytical methods, the model used is that of (Hickling, 1964), since this paper displays the spectra of scattered pressure from spherical shells in a liquid medium, which expedite the checking of the programming code that had to be developed. (Hickling, 1964) highlighted that; *the structure of sonar echoes is strongly dependent on the vibrations induced in the target by the incident sound.* To realistically estimate the scattering, this model solves the vector wave equation in the region occupied by the solid to take these vibrations into account. The analytical procedures used for this purpose are based on the well-established method of separation of variables, which can be successfully applied to the sphere geometry for modelling such parameters as the elastic properties of the material and shell thickness.

The scattered sound pressure is expressed as an infinite sum of modes, each of which corresponds to a particular directionality of vibration of the sphere (for example, the *n*=0 mode is the "breathing" mode). For the present scenario, back-scattering is assumed; the angle θ from the incoming plane wave to the chosen direction of scattering is assumed to be 180° (π). The main formula used was Eq. (8) in (Hickling, 1964), which yields the sound pressure, p_s, scattered to range, r, from the shell:

$$p_s(r,\theta) = \frac{P_0}{kr} \sum_{n=0}^{N}(2n+1) \, P_n(\cos\theta) \, c_n \, exp(ikr - i\omega t), \tag{6}$$

where P_0 and k are the pressure amplitude and wavenumber of the incident plane wave, the P_n are the Legendre polynomials, and N is the actual number of modes summed, determined as the minimum number such that partial sums of higher modes are negligible. The modal coefficients c_n are obtained by defining acoustic and elastic waves in the fluid and solid media and obtaining amplitudes of each from the boundary conditions at the inner and outer radii of the shell. Hickling's model is an exact implementation of the theory of elasticity; it is not a thin-shell theory. It automatically includes effects such as creeping waves and Lamb waves that were highlighted during subsequent decades. The expression for each c_n includes the ratio of the determinants of two matrices, each element of which contains spherical Bessel functions, spherical Neumann functions, and their derivatives. The (short) computation times of analytical models such as Hickling's are independent of the range, but a short range of 0.5 m was selected in order that the numerical Finite-Element model to also be applied could produce spectra within a reasonable time. In general, the amplitude of the scattered wave is given by the spherical Hankel function which, as range increases beyond many wavelengths, asymptotes to spherical spreading. The above expression depicts spherical spreading, which becomes more accurate with increasing frequency; as frequency increases from 10 to 20 kHz the number of wavelengths in a distance of 0.5 m increases from 3.3 to 6.7. This simplification was made to be consistent with the numerical model model.

We consider a finite number of modes in the model, which is increased until our results converge. During the initial increase of mode number (from 0 to 10, say) the amplitudes of the modes can vary in a quasi-random manner. At a later stage they begin to decay steadily with further increase, and when the amplitude of a mode in that stage becomes negligible in relation to the mode sum then the sum can be terminated without loss of accuracy. It was found in the present cases that a maximum mode number of 30 was generally sufficient in that regard.

In (Hickling, 1964), it was noted that potential problems may arise in the numerical evaluation of the series expansion used to calculate the backscattered pressure from the sphere due to the overflow and underflow limits of one's computer. This problem may arise because the arguments of the Bessel functions differ in magnitude, meaning the products of the elements in the determinants can easily reach the overflow and underflow limits before a sufficient number of terms in the series expansion have been evaluated. To avoid this computational limit, the elements in the determinant were arranged so that the terms in the expansion were products alternately of the Bessel and the Neumann functions. This was done because with an increase in the subscript n, the Neumann functions increase whereas the Bessel functions decrease, therefore, the growth of the Neumann functions was used to neutralise the diminution of the Bessel functions. In the present calculations Hickling's procedure was not used; instead, a "quadruple" precision was used for the arithmetic. This resulted in satisfactory accuracies in the present case (albeit with longer run times), as will be seen by the absence of noise in the results, and good agreement with the results from the numerical procedure (which did not use Bessel functions of any type).

3   SCATTERING FROM AIR FILLED/VACUOUS SPHERICAL SHELLS

In this section, the pressure scattered from three different *empty* spherical shells is evaluated when subject to a number of incident plane waves sweeping from 1 kHz to 20 kHz, in steps of 20 Hz. Assuming the waves are incident from directly above the shell, the scattered responses are evaluated at the zenith, at 0.5 m from the target. Both analytical and numerical methods are used to evaluate the back scatter and the results are compared when each target is surrounded by either seawater or water-saturated sand.

Figure 2 shows the scattered pressure from the three spheres defined in Table 1, plotted in dB re. the amplitude of the incident plane wave, when surrounded by seawater and a water saturated sand domain. The results from the numerical model are plotted along with the results obtained via the analytical model, for comparison. To begin with, from all plots presented in Figure 2, the modal behaviour of the spherical shells can clearly be seen. Each geometry exhibits several unique resonant peaks which may be exploited during target classification to characterise each object. Further, these plots also demonstrate the strong agreement between the numerical and analytical results, with all resonance frequencies accurately identified and most of the pressure level aligning accurately. However, some small differences in the pressure level are observed, in particular off resonance and towards the upper end of the presented frequency range. In the following, when comparing the scattering for each case the discussion will refer to the numerical results as these are typically used for modelling MCM databases.

The plot in Figure 2.a) shows the scattering from Sphere $_{50,1}$ when surrounded by seawater, plotted along with the scattering when surrounded by water-saturated sand. From this plot it can be seen that when the surrounding domain changes from seawater to saturated sand, the resonances shift down in frequency. The first and most strongly scattering resonance shifts down from approximately 6.7 kHz to 5.5 kHz and the relative pressure level remains unchanged, albeit appearing less damped when surrounded by saturated sand. The second resonance shifts down from approximately 8.4 kHz to 6.9 kHz, and reduces in level by approximately 7 dB. All subsequent, higher frequency resonances are heavily damped. Additionally, when the shell is surrounded by saturated sand, a large anti-resonance occurs at approximately 17 kHz, which is not present when surrounded by seawater.

Figure 2.b) shows the scattering from Sphere $_{50,0.55}$ when surrounded by seawater, plotted along with the scattering when surrounded by water-saturated sand. Sphere $_{50,0.55}$ has a thinner shell thickness than Sphere $_{50,1}$, as a result the resonance frequencies of Sphere $_{50,0.55}$ are lower than the corresponding resonances of Sphere $_{50,1}$, in each domain. The first two most strongly scattering resonances occur at 5.6 kHz and 7 kHz when the shell is surrounded by seawater, and 4.4 kHz and 5.6 kHz when surrounded by saturated sand. Additionally, a large antiresonance is observed in the scattering spectrum of Sphere $_{50,0.55}$ when surrounded by seawater which is not present in the spectrum of Sphere $_{50,1}$ when the outer domain is seawater. In general, when changing the outer domain from seawater to saturated sand, the trends observed for Sphere $_{50,1}$ are also observed for Sphere $_{50,0.55}$. When moving from seawater to saturated sand, the first and most strongly scattering resonance is largely unaffected, however, appearing more highly damped. The second resonance reduces in level by approximately 10 dB and all other higher frequency resonances are heavily damped. Further, the large antiresonance at approximately 16 kHz, shifts up in frequency to approximately 17.5 kHz when moving from seawater to saturated sand.

Finally, Figure 2.c) shows the scattering from Sphere $_{100,1}$ when surrounded by seawater, along with the scattering when surrounded by saturated sand. Sphere $_{100,1}$ has a larger diameter than Sphere $_{50,1}$, however, the shell thickness remains constant. From these results, it can be seen that the strongest scattering resonance decreases in frequency, when compared to Sphere $_{50,1}$, to approximately 2.7 kHz when surrounded by seawater and 2.1 kHz when surrounded by saturated sand. The second resonance shifts from 3.4 kHz in seawater to 2.7 kHz in saturated sand and the relative pressure level of the first two resonances decrease by approximately 8 dB. All higher frequency resonances are heavily damped and not visible when surrounded by saturated sand. These results also show two large antiresonances in the scattering response when surrounded by both seawater and saturated sand. The lower of the two antiresonances shifts up from 7.8 kHz to 8.6 kHz and the higher moves down from 18.9 kHz to 18.6 kHz.
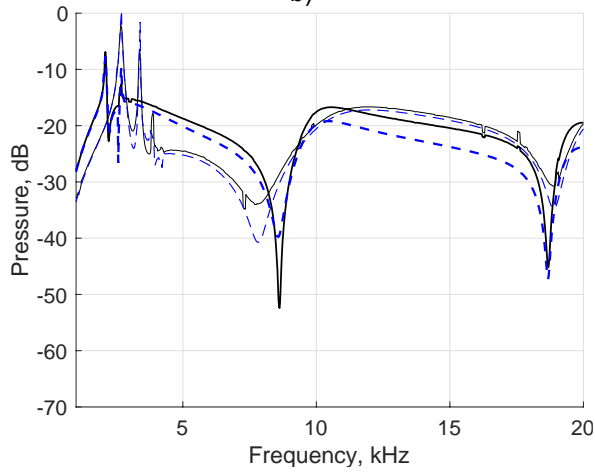
In general, this study has shown that only the two most strongly scattering resonances of each target remain present in the spectra, typically shifted down in frequency, when the outer domain of the target changes from seawater to water-saturated sand, whilst less strongly scattering, higher frequency, resonances disappear.
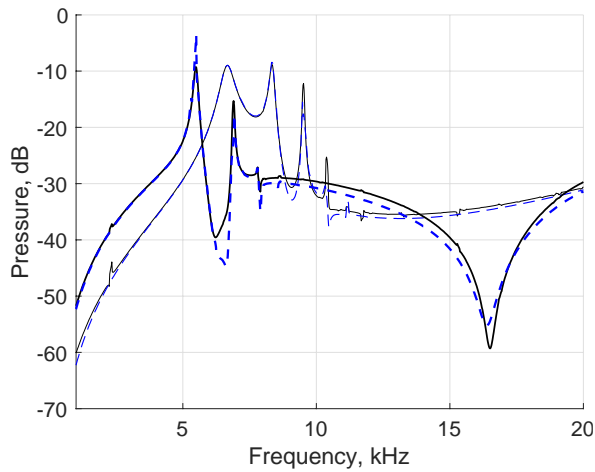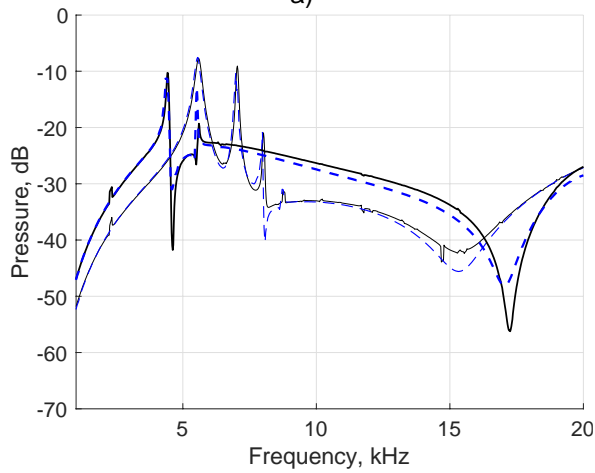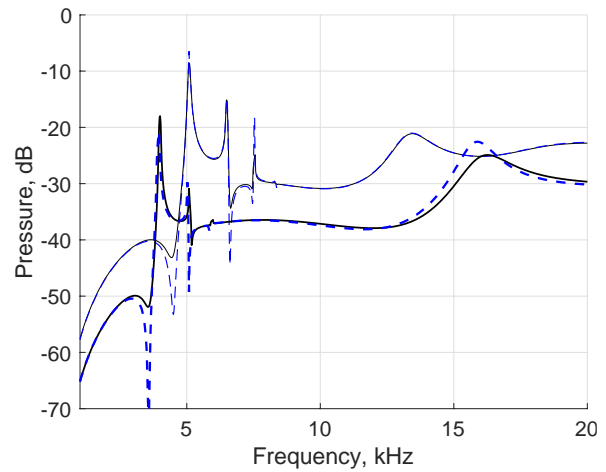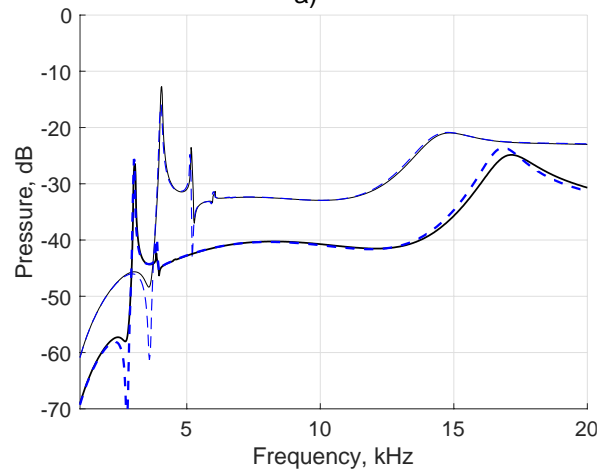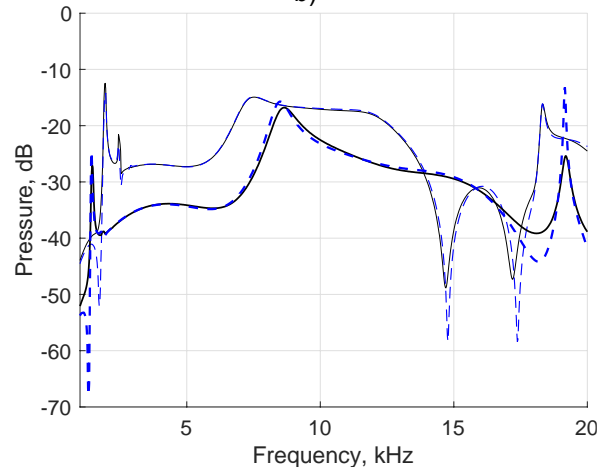
Figure 2. Scattered pressure evaluated 0.5 m above the air filled (numerically modelled – solid black lines) and vacuous (analytically modelled – dashed blue lines) spherical shells surrounded by a seawater medium (thin lines) and a saturated sand medium (thick lines). The plot in subfigure a) shows the back scatter from Sphere $50,1$, b) shows the back scatter from Sphere $50,0.55$ and c) shows the back scatter from Sphere $100,1$.

Figure 3. Scattered pressure evaluated 0.5 m above the *full* spherical shells surrounded by seawater (thin lines) and saturated sand medium (thick lines). The solid black lines show the results obtained using a numerical model and the dashed blue lines show the results obtained using the analytical model. The plot in subfigure a) shows the back scatter from Sphere $50,1$, b) shows the back scatter from Sphere $50,0.55$ and c) shows the back scatter from Sphere $100,1$.

4 SCATTERING FROM WATER AND SATURATED SAND FILLED SHELLS

In this section, the pressure scattered by the three spherical shells defined in Table 1 is evaluated when subject to the excitation as described in Section 3. However, in the following, the inner domain of the shell is modelled using the same properties as the outer domain. As in Section 3, the scattered responses are evaluated at 0.5 m from each target and the results are compared when each shell is surrounded and filled with either, seawater or saturated sand.

The plots in Figure 3 show the pressure scattered from the three spherical shells defined in Table 1, plotted in dB re. the amplitude of the incident plane wave, when filled and surrounded by seawater, and saturated sand domains. As in Section 3, the results from the analytical and numerical models are plotted together for comparison, and demonstrate the strong agreement between the analytical and numerical models. Many of the same observations can be made for these results as were made for the results in Figure 2. That is, the scattering responses clearly show the modal behaviour of the spherical shells, each exhibiting a unique set of resonances. These resonances can be split into two distinct types; the lightly damped lower frequency resonances and heavily damped higher frequencies. In general, it can be seen that when changing the inner and outer domains from seawater to saturated sand, the lightly damped lower frequency resonances decrease in both frequency and relative pressure level, as was observed in Section 3, whereas the more heavily damped higher frequency resonances increase in frequency whilst remaining a constant level. Further, comparing these results to the equivalent results for *empty* shells in Figure 2, it can be seen that the lightly damped lower frequency resonances presented in Figure 3 for the *full* shells, appear at lower frequencies than in that the *empty* shells.

Figure 3.a) shows the scattering from Sphere $_{50,1}$ when filled and surrounded by seawater, plotted along with the scattering when filled and surrounded by saturated sand. Changing the inner and outer domain of Sphere $_{50,1}$ from seawater to saturated sand results in the first two resonances decreasing in level by approximately 10 and 14 dB, respectively, and shifting down in frequency from 5 kHz and 6.5 kHz to 4 kHz and 5 kHz, respectively. Lastly, the third resonance at 7.5 kHz all but disappears after a reduction in level by 20 dB, and the resonance at approximately 13.5 kHz shifts up to 16 kHz.

The plot in Figure 3.b) shows the scattering from Sphere $_{50,0.55}$ when filled and surrounded by seawater, plotted along with the scattering when filled and surrounded by saturated sand. As observed in the previous section, for the lightly damped lower frequency resonances, a reduction in the frequency and relative pressure level is observed when changing domains from seawater to saturated sand. The first two resonances decrease in level by approximately 13 and 16 dB, respectively, and shift down in frequency from 4 kHz and 5.1 kHz to 3 kHz and 3.9 kHz, respectively. The third resonance at 6 kHz disappears and the heavily damped resonance at approximately 14.6 kHz shifts up to 17.2 kHz.

Finally, Figure 3.c) shows the scattering from Sphere $_{100,1}$ when filled and surrounded by seawater, along with the scattering when filled and surrounded by saturated sand. From these results it can be seen that the first resonance decreases in frequency from 1.9 kHz to 1.4 kHz, and reduces in level by 12 dB when the inner and outer domains are changed from seawater to saturated sand. Further, the second resonance at 2.4 kHz disappears, whilst the resonance at 7.5 kHz increases in frequency to 8.7 kHz. Lastly, the resonance at 18.3 kHz increases to 19 kHz and two large antiresonances are introduced in the scattering response at 14.7 kHz and 17.3 kHz when the inner and outer domains are modelled as saturated sand.

As in Section 3, this study has shown that typically only the most strongly scattering resonances of each target remain present in the spectra, as would be expected, when the outer domain of the target changes from seawater to water-saturated sand. However, in this case higher frequency features are also introduced into the spectra which tend to shift up in frequency when the outer domain of the target changes from seawater to water-saturated sand.

5 CONCLUSIONS

The work in this paper has investigated the effect of underwater burial on the resonant behaviour of three geometrically different spherical shells where the inner domain is modelled as either, *empty* or *full* (inner domain and outer domain have matching material properties). This study has considered two acoustic domains, seawater and saturated sand. The backscatter from the shell was evaluated, both numerically and analytically as an incident, low frequency pulse train was used to ensonify each domain. The results have shown that each target exhibits unique resonant behaviour when excited by the pulse, which is crucial for effective target classification during MCM operations. Also shown is how the frequency and relative level of the resonances change when the external domain changes. For the three spherical shells studied in this paper, in general, the lower frequency,

lightly damped resonances decrease in both frequency and relative level when the external medium changes from seawater to saturated sand, whereas higher frequency features, such as antiresonances and heavily damped resonances, tend to increase in frequency. Further, when the inner domain of the shells changes to match the outer domain, the lightly damped lower resonance frequencies of the back scatter decrease in frequency when compared to the equivalent resonances of the *empty* shells, and large heavily damped resonances are introduced at higher frequencies. Based on the results presented in this study, it has been shown that as the internal and external domains of a spherical shell change, the features of the scattering spectra change in a somewhat predictable manner. However, it should be emphasised that this initial study was designed to validate a numerical modelling capability and inform the next steps of a longer-term project, for more complex and realistic geometries the effects of burial and other changes may not be so obvious. Moving forward, further work will look to utilise the models presented in this study to create a database of test sonar signals. This database will then be used to develop novel signal processing schemes that are able to extract common features from sonar signals, which can be related directly to a specific target, regardless of position in the water column or below the seabed.

ACKNOWLEDGEMENTS

REFERENCES

Bjørnø, L. (2017). *Applied Underwater Acoustics.* UltraTech Holding, Taastrup, Denmark: Elsevier.

Burnett, D.S. (2015). "Computer Simulation for Predicting Acoustic Scattering from Object at the Bottom of the Ocean." *Acoustics Today,* vol. 11, no. 1, pp. 28 - 36.

Flax, H.L.P., and Neubauer, W.G. (1978). "Reflections of elastic waves by a cylindrical cavity in an absoptive medium." *Journal of the Acoustical Society of America,* vol. 63, pp. 675 - 680. https://doi.org/10.1121/1.381793

Hall, M. (1975). "Bulk modulus of a fluid-filled spherical shell." *Journal of the Acoustical Society of America*, vol. 57, no. 2, pp. 508 - 510. https://doi.org/10.1121/1.380439

Hickling, R. (1964). "Analysis of Echoes from a Hollow Metallic Sphere in Water." *Journal of the Acoustical Society of America*, vol. 36, pp. 1124 - 1137. https://doi.org/10.1121/1.1919173

Langner, F., Knauer, C., Jans, W. and Ebert, A. (2009). "Side scan sonar image resolution and automatic object detection, classification and identification." *OCEANS.* Bremen. pp. 1 - 8. 10.1109/OCEANSE.2009.5278183

Le, H.T., Phung, S.L., Chapple, P.B., Bouzerdoum, A., Ritz, C.H. and Tran, L.C. (2020). "Deep Gabor neural network for automatic detection of mine-like objects in sonar imagery." *IEEE Access*, vol. 8, no. 1, pp. 94126 - 94139. 10.1109/ACCESS.2020.2995390

Maguer, A., Fox, W.L.J., Schmidt, H., Poliquen, E. and Bovio, E. (2000). "Mechanisms for subcritical penetration into a sandy bottom: Experimental and modeling results." *Journal of the Acoustical Society of America, vol.* 107, pp. 1215 - 1225. https://doi.org/10.1121/1.428411

Naval Research Council. (2001). *Naval Mine Warefare: Operational and Technical Challenges for Naval Forces.* Washington, DC: The National Academies Press.

Tesei, A., Fox, W.L.J., Maguer, A. and Løvik, A. (2000). "Target parameter estimation using resonance scattering analysis applied to air-filled, cylindical shalled in water." *Journal of the Acoustical Society of America*, vol. 108, pp. 2891 - 2900. https://doi.org/10.1121/1.1312359